Synthesis and Characterization of a Novel Arginine-Grafted Dendritic Block Copolymer for Gene Delivery and Study of Its Cellular Uptake Pathway Leading to Transfection

ARTICLE *in* BIOCONJUGATE CHEMISTRY · MARCH 2007

Impact Factor: 4.51 · DOI: 10.1021/bc0601525 · Source: PubMed

6 AUTHORS, INCLUDING:

Tae-Il Kim
Seoul National University
34 PUBLICATIONS **1,286** CITATIONS
SEE PROFILE

Joon Sig Choi
Chungnam National University
71 PUBLICATIONS **2,200** CITATIONS
SEE PROFILE

Synthesis and Characterization of a Novel Arginine-Grafted Dendritic Block Copolymer for Gene Delivery and Study of Its Cellular Uptake Pathway Leading to Transfection

Tae-il Kim,[†] Jung-un Baek,[†] Jae Keun Yoon,[†] Joon Sig Choi,[‡] Kwan Kim,[†] and Jong-sang Park*[,†]

School of Chemistry and Molecular Engineering, Seoul National University, San 56-1, Shillim-dong, Gwanak-gu, Seoul 151-742, and Department of Biochemistry, Chungnam National University, 220 Gung-dong, Yuseong-gu, Daejeon 305-764, Korea. Received June 2, 2006; Revised Manuscript Received November 29, 2006

We synthesized a novel arginine-grafted dendritic block copolymer, R-PAMAM-PEG-PAMAM-R G5 (PPP5-R) for gene delivery systems. Its Mw was measured as 2.74×10^4 Da by MALDI-TOF, and approximately 36 arginine residues are found to be grafted to the polymer by ^{1}H NMR. PPP5-R was able to form polyplexes with plasmid DNA, the average size of which was about 200 nm. Positive ζ-potential values (+22 to +28 mV) of PPP5-R polyplex indicate the formation of positively charged stable polyplex particles and suggest that large dendritic blocks with high positive charge may not be fully shielded by PEG chains even after PEG-coated complex formation. PPP5-R polyplex shows enhanced water solubility due to the polymer's PEG core and also shows low cytotoxicity, representing the potential for in vivo application. We identified the greatly enhanced transfection efficiency of PPP5-R in comparison with that of native PPP5 on various cell lines. Moreover, in view of the result of various cellular uptake inhibitor treatments during a transfection step, the cellular uptake of PPP5-R polyplex leading to effective transfection is thought to be not dependent on one exclusive pathway and to have the possibility of multiple pathways (caveolae-, clathrin-, and macropinocytosis-mediated pathways), contrary to the caveolae-dependent uptake of the PPP5 polyplex lacking arginine residues.

INTRODUCTION

The necessity of developing efficient gene delivery carriers is increasing gradually both in basic sciences and in clinical research fields. Viral vectors (adenoviruses, adeno-associate viruses, retroviruses, etc.) have been successfully applied to various clinical tests for gene therapy because of their high gene delivery efficiency, but their side effects such as severe pathogenicity occasionally limited further application (*1*). On the other hand, nonviral vectors have been studied as alternatives to viral vectors because of their lower cytotoxicity, nonimmunogenicity, more convenient handling, and larger capacity of gene to deliver (*2*−*4*).

However, nonviral vectors including cationic polymers and lipids show much lower transfection efficiency than viral vectors. They also need to overcome the barriers of considerable polyplex aggregation due to the decreased water solubility induced by charge neutralization through the electrostatic interaction between polycationic vectors and polyanionic DNA (*5*).

Our recent report suggested PAMAM-PEG-PAMAM (PPP[1]) as a novel triblock dendritic polymeric vector (*6*). PPP could form polyplexes with plasmid DNA showing much enhanced water solubility. However, the polymer did not show satisfactory transfection efficiency in vitro experiments, urging us to improve the efficiency of the polymer. Recently, Tat-mediated molecular delivery into cells was highlighted and is the subject of intensive research (*7*−*9*). Arginine residues of Tat peptide are thought to perform an important role for the intracellular translocation of molecular delivery (*10*). Also, the synthetic lipidic vectors with a guanidinium headgroup of arginine showed great potential for a gene delivery system (*11*). Moreover, we recently reported that the arginine conjugation of PAMAM dendrimer surfaces led to highly enhanced transfection efficiency of the polyplex (*12*). So, we designed a novel dendritic polymeric vector by conjugating arginine residues to the periphery of PPP in order to increase the transfection efficiency of the polymer, keeping the good water solubility.

Here, we report the synthesis of R-PAMAM-PEG-PAMAM-R (PPP-R), characterization of its self-assembly with plasmid DNA, and its transfection results in vitro.

Meanwhile, the cellular uptake mechanism of cell-penetrating peptides containing arginine residues was reported by many groups (*13*−*15*). However, the cellular uptake mechanism of arginine-grafted dendritic polymer/DNA complex leading to effective transfection has not been reported yet. So, we also report the cellular uptake pathway of PPP-R polyplex by comparing with that of PPP polyplex lacking arginine residues for the first time.

EXPERIMENTAL SECTION

Materials. Poly(ethylenimine) (25 kDa), methyl acrylate, ethylenediamine, *N*,*N*-diisopropylethylamine (DIPEA), piperidine, 3-[4,5-dimethylthiazol-2-yl]-2,5-diphenyltetrazolium bromide (MTT), 2,5-dihydroxybenzoic acid (DHB), and fucose were purchased from Sigma-Aldrich (St. Louis, MO). Poly(ethylene glycol)-*bis*-amine (MW 3400) was purchased from Shearwater Polymers (Huntsville, AL). *N*-Hydroxybenzotriazole (HOBt) and 2-(1*H*-benzotriazole-1-yl)-1,1,3,3-tetramethyluro-

* Corresponding author. Jong-sang Park, Ph.D. Phone: 82-2-880-6660. Fax: 82-2-877-5110. E-mail: pfjspark@plaza.snu.ac.kr.

† Seoul National University.

‡ Chungnam National University.

[1] Abbreviations: PAMAM, poly(amido amine); PEG, poly(ethylene glycol); PPP, PAMAM-PEG-PAMAM; PPP-R, Arg-PAMAM-PEG-PAMAM-Arg; PEI, polyethylenimine; DHB, 2,5-dihydroxybenzoic acid; HOBt, *N*-hydroxybenzotriazole; HBTU, 2-(1*H*-benzotriazole-1-yl)-1,1,3,3-tetramethyluronium hexafluorophosphate; pbf, 2,2,4,6,7-pentamethyldihydrobenzofuran-5-sulfony; MALDI-TOF, matrix assisted laser desorption ionization-time of flight; AFM, atomic force microscopy; PBS, phosphate buffered saline; PLLD, poly(L-lysine) dendrimer.

10.1021/bc0601525 CCC: $37.00
Published on Web 02/23/2007

Scheme 1. Synthetic Scheme of PPP5-R

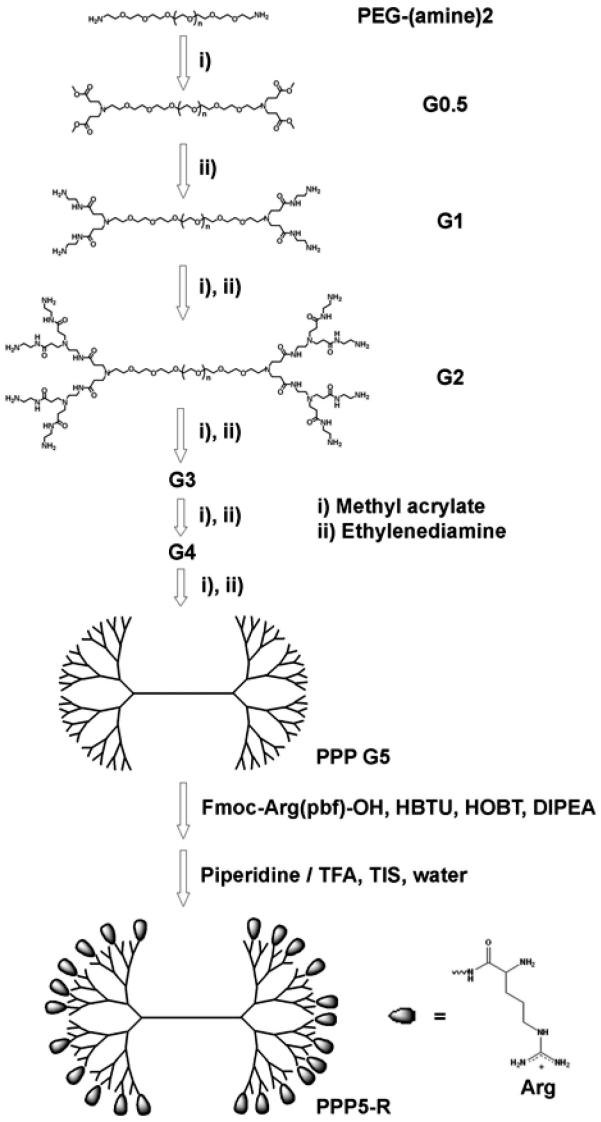

nium hexafluorophosphate (HBTU) were purchased from Anaspec, Inc. (San Jose, CA). Fmoc-L-Arg(pbf)-OH was purchased from Novabiochem (San Diego, CA). Luciferase 1000 Assay System and Reporter Lysis Buffer were purchased from Promega (Madison, WI). The luciferase expression plasmid, pCN-Luci, was constructed by subcloning cDNA of *Photinus pyralis* luciferase with the 21-aminoacid nuclear localization signal from SV40 large T antigen to pCN (*16*). The GFP expression plasmid, pEGFP-N3 (4.7 kb), was purchased from BD Biosciences Clontech (Mountain View, CA). PicoGreen reagent was purchased from Molecular Probes (Eugene, OR). Fetal bovine serum (FBS), minimal essential medium (MEM), and Dulbecco's modified Eagle's medium (DMEM) were purchased from GIBCO (Gaithersburg, MD). The Micro BCA protein assay kit was purchased from Pierce (Rockford, IL). All other chemicals were purchased and used without any further purification.

Synthesis of PPP5-R. The backbone polymer, PAMAM-PEG-PAMAM G5 (PPP5) was synthesized according to the methods of our previous work (*6*). Briefly, PPP5 was synthesized using poly(ethylene glycol)-*bis*-amine(PEG) (MW 3400) as a polymeric supporter through iterative multistep reactions of Michael addition of methyl acrylate (step 1) followed by amidation of ethylenediamine (step 2) as shown in Scheme 1.

Synthesis of PPP0.5 (step 1). First, PEG was dissolved in methanol and added dropwise to 100 equiv of methyl acrylate kept at 37 °C. After 48 h, methanol and unreacted methyl acrylate were removed under vacuum. The residue was precipitated with an excess of cold ethyl ether and dried under vacuum to remove ethyl ether, leaving a white solid, PAMAM-PEG-PAMAM G 0.5 (PPP0.5). ^{1}H NMR (MeOD): δ PEG(CH_2CH_2O) = 3.63; δ PAMAM($-COOCH_3$) = 3.66; δ PAMAM($-CH_2COOCH_3$) = 2.51; δ PAMAM(protons next to tertiary amines) = 2.85.

Synthesis of PPP1 (step 2). PPP0.5 was dissolved in methanol and added dropwise to 100 equiv of ethylenediamine kept at 37 °C. After 48 h, methanol and ethylenediamine were removed under vaccum. The residue was precipitated with an excess of ethyl ether to remove residual ethylenediamine and dried under vacuum to remove ethyl ether, leaving a pale yellow solid, PAMAM-PEG-PAMAM G 1.0 (PPP1). ^{1}H NMR (D_2O): δ PEG(CH_2CH_2O) = 3.72; δ PAMAM($-CH_2CONH-$) = 2.46; δ PAMAM($-CONHCH_2-$) = 3.32; δ PAMAM(protons next to amines) = 2.6−3.0.

Synthesis of PPP1.5−PPP5. Steps 1 and 2 were consecutively repeated to obtain the higher-generation copolymers. Synthesis of higher-generation copolymer is identical to the above methods, and so we omit them and show the ^{1}H NMR result of each generation copolymer.

Synthesis of PPP1.5. ^{1}H NMR (MeOD): δ PEG(CH_2CH_2O) = 3.63; δ PAMAM($-COOCH_3$) = 3.67; δ PAMAM($-CONHCH_2-$) = 3.27; δ PAMAM($-CH_2COOCH_3$) = 2.46; δ PAMAM($-CH_2CONH-$) = 2.39; δ PAMAM(protons next to tertiary amines) = 2.6−3.0.

Synthesis of PPP2. ^{1}H NMR (D_2O): δ PEG(CH_2CH_2O) = 3.72; δ PAMAM($-CH_2CONH-$) = 2.45; δ PAMAM($-CONHCH_2-$) = 3.31; δ PAMAM(protons next to amines) = 2.6−3.0.

Synthesis of PPP2.5. ^{1}H NMR (MeOD): δ PEG(CH_2CH_2O) = 3.63; δ PAMAM($-COOCH_3$) = 3.67; δ PAMAM($-CONHCH_2-$) = 3.26; δ PAMAM($-CH_2COOCH_3$) = 2.46; δ PAMAM($-CH_2CONH-$) = 2.39; δ PAMAM(protons next to tertiary amines) = 2.6−3.0.

Synthesis of PPP3. ^{1}H NMR (D_2O): δ PEG(CH_2CH_2O) = 3.72; δ PAMAM($-CH_2CONH-$) = 2.46; δ PAMAM($-CONHCH_2-$) = 3.36; δ PAMAM(protons next to amines) = 2.6−3.0.

Synthesis of PPP3.5. ^{1}H NMR (MeOD): δ PEG(CH_2CH_2O) = 3.68; δ PAMAM($-COOCH_3$) = 3.71; δ PAMAM($-CONHCH_2-$) = 3.30; δ PAMAM($-CH_2COOCH_3$) = 2.51; δ PAMAM($-CH_2CONH-$) = 2.43; δ PAMAM(protons next to tertiary amines) = 2.6−3.0.

Synthesis of PPP4. ^{1}H NMR (D_2O): δ PEG(CH_2CH_2O) = 3.72; δ PAMAM($-CH_2CONH-$) = 2.46; δ PAMAM($-CONHCH_2-$) = 3.31; δ PAMAM(protons next to amines) = 2.6−3.0.

Synthesis of PPP4.5. ^{1}H NMR (MeOD): δ PEG(CH_2CH_2O) = 3.66; δ PAMAM($-COOCH_3$) = 3.69; δ PAMAM($-CONHCH_2-$) = 3.28; δ PAMAM($-CH_2COOCH_3$) = 2.48; δ PAMAM($-CH_2CONH-$) = 2.41; δ PAMAM(protons next to tertiary amines) = 2.5−3.0.

Synthesis of PPP5. ^{1}H NMR (D_2O): δ PEG(CH_2CH_2O) = 3.72; δ PAMAM($-CH_2CONH-$) = 2.45; δ PAMAM($-CONHCH_2-$) = 3.31; δ PAMAM(protons next to amines) = 2.6−3.0.

Synthesis of PPP5-R. Arginine coupling to the PPP5 was performed in anhydrous DMF for 1 day at room temperature with 4 equiv of HOBT, HBTU, and Fmoc-Arg(pbf)-OH and 8 equiv of DIPEA. The product was precipitated with an excess of diethyl ether three times and mixed with an equal volume of piperidine (30% in DMF) at room temperature for 20 min to remove the Fmoc groups of coupled Fmoc-Arg(pbf)-OH. The reaction mixture was precipitated again with diethyl ether and

the reagent (95:2.5:2.5, trifluoroacetic acid/triisopropylsilane/water, v/v) was used to deprotect the pbf groups of coupled arginine residues at room temperature for 6 h. After the reaction, the final product, PPP5-R, was dialyzed against ultrapure water overnight and lyophilized before use for analysis and assay.

^{1}H NMR (D_2O): δ arginine($-HCCH_2C\mathbf{H_2}CH_2NH-$) = 1.66; δ arginine($-HCC\mathbf{H_2}CH_2CH_2NH-$) = 1.86; δ PAMAM($-C\mathbf{H_2}$-$CONH-$) = 2.50; δ PAMAM(protons next to amines) = 2.7−2.9; δ arginine($-HCCH_2CH_2C\mathbf{H_2}NH-$) = 3.24; δ PAMAM($-CONHC\mathbf{H_2}-$ and $-CONHCH_2C\mathbf{H_2}NHCO-$) = 3.37; δ PEG($-C\mathbf{H_2}C\mathbf{H_2}O-$) = 3.71; δ arginine($-\mathbf{H}CCH_2CH_2CH_2NH-$) = 3.86.

^{1}H NMR Spectroscopy. ^{1}H NMR spectra of the polymers were obtained using a Bruker DPX-300 NMR spectrometer (300 MHz). For analysis, the polymer samples were dissolved in MeOD or D_2O containing 3-(trimethylsilyl)propionic-2,2,3,3-d_4 acid sodium salt as an internal reference (0 ppm).

MALDI-TOF Mass Spectroscopy. MALDI-TOF mass spectra were obtained using a Voyager-DE STR Biospectrometry Workstation (Applied Biosystems, Inc.) in the linear delayed-extraction mode. A polymer solution was prepared by dissolving 1 mg of the polymer in 1 mL of water. The matrix solution was prepared by dissolving 10 mg of matrix (DHB/fucose = 1:1) in 1 mL of the 1:1 mixture of the water and acetonitrile. The samples were prepared by mixing them to a final volume of 2 μL at various ratios.

Gel Retardation Assays. PPP5-R/plasmid complexes at various weight ratios ranging from 0.5 to 8.0 were prepared in Hepes buffered saline (10 mM Hepes, 1 mM NaCl; pH 7.4). After 30 min incubation at room temperature for the complex formation, the samples were electrophoresed on a 0.7% (w/v) agarose gel and stained in an ethidium bromide solution (0.5 μg/mL), and analyzed on a UV illuminator to show the location of the DNA.

Polymer/DNA Self-Assembly Analysis by PicoGreen Assay. PicoGreen assay was carried out to analyze the self-assembly of PPP5-R/plasmid DNA quantitatively as reported recently (*12*, *16*). Briefly, PicoGreen reagent (200×) was diluted to 200-fold in TE buffer before the experiment. 200 μL of the diluted PicoGreen stock solution was mixed with the same volume of blank solution or polyplex solution (1 μg DNA, 1× HBS) prepared at various weight ratios ranging from 0 to 10. After 2 min incubation, each solution was added to 1.6 mL of TE buffer in a test tube. Fluorescence was measured with a FP-750 spectrofluorometer (Jasco) at room temperature. Excitation and emission wavelengths were set at 480 and 520 nm, respectively. Values were represented as relative fluorescence (%) to the value of plasmid DNA.

Polyplex Size Measurements. The hydrodynamic diameters of the PPP5-R/plasmid DNA complexes were determined by light scattering. 2 mL of polyplex solutions containing 5 μg of DNA were prepared at various weight ratios ranging from 1 to 20. After 30 min incubation, polyplex sizes were measured using a Zetasizer 3000HS (Malvern Instruments, U.K.). The laser used is a nominal 5 mW HeNe laser having a 633 nm wavelength. Scattered light was detected at a 90° angle. The refractive index (1.33) and the viscosity (0.89) of ultrapure water were used at 25 °C for measurements. *Zetasizer 3000 (Advanced) Size Mode* v1.61 software was used for data acquisition. Data analysis was performed in automatic mode. Measured sizes were presented as the average values of five runs.

ζ-Potential Measurements. 2 mL of polyplex solutions containing 5 μg of DNA were prepared in Hepes buffered saline (10 mM Hepes, 1 mM NaCl; pH 7.4) at various weight ratios ranging from 0.5 to 20. After 30 min incubation, each polyplex solution was diluted to a 10 mL final volume prior to measurements. ζ-Potential measurements were carried out using a Zetasizer 3000HS (Malvern Instruments, U.K.) at 25 °C. *Zetasizer 3000 (Advanced) Zeta Mode* v1.61 software was used for data acquisition. The sampling time was set to automatic. Potential values were presented as the average values of five runs.

Atomic Force Microscopy (AFM). The particle shapes and sizes of the polymer/plasmid DNA complexes were analyzed using atomic force microscopy (Nanoscope IIIa system, Digital Instruments, Inc., Santa Barbara, CA). The samples were prepared by mixing 0.1 μg of plasmid DNA with aqueous polymer solution at various weight ratios to obtain a final DNA concentration of 10 ng/μL. After 30 min incubation, 1 μL aliquots of the complex solutions were placed on a freshly cleaved mica surface and allowed to stick for 1−2 min. Excess solution was removed by careful absorption onto filter paper, and the mica surface was further dried at room temperature for 24 h. The image mode was set to tapping mode, and the scanning speed was 1−5 Hz.

Polyplex Solubility Measurements in Water. The solubility of polyplex was evaluated by the method developed by Wadhwa et al. with a slight modification (*17*). The PAMAM-R G 4 dendrimer was used as a control reagent (*12*). Polymers were mixed with 20 μg of plasmid DNA at various weight ratios in 0.5 mL of 25 mM Hepes buffer. After incubation for 30 min at room temperature, each mixture was centrifuged for 5 min at 13000 rpm and 10 °C. Then, the absorbance of each supernatant was measured at 260 nm. The solubility was calculated as a percentage ratio of the absorbance of pure DNA solution and each supernatant.

Cytotoxicity Assay. The cytotoxicity of the polymers was measured by MTT assay. HepG2 human hepatocellular carcinoma cells were seeded in a 96-well tissue culture plate at 10^4 cells per well in 90 μL MEM medium containing 10% FBS. Cells achieving 70−80% confluence after 24 h were exposed to 10 μL of the polymer solutions having various concentrations for 24 h. Then, 26 μL of stock solution of MTT (2 mg/mL in PBS) were added to each well. After 4 h of incubation at 37 °C, each medium was removed, and 150 μL of DMSO was added to each well to dissolve the formazan crystal formed by proliferating cells. Absorbance was measured at 570 nm using a microplate reader (Molecular Devices Co., Menlo Park, CA) and recorded as a percentage relative to the value of untreated control cells.

In Vitro Transfection. HepG2, HeLa human adenocarcinoma cells were seeded at a density of 5×10^4 cells/well in a 24-well plate in a medium containing 10% FBS and grown to reach 70−80% confluence prior to transfection. C2C12 mouse myoblast cells were seeded at a density of 3×10^4 cells/well. Before transfection, the cells were rinsed with PBS, and serum-free or serum-containing medium was added to each well. The cells were treated with polyplex solution containing 2 μg of plasmid DNA at different weight ratios for 4 h at 37 °C. In the presence of serum, the cells were incubated for 24 h after transfection. After exchange of medium, cells were further incubated for 2 days after transfection. Then, the growth medium was removed, and the cells were rinsed with PBS and shaken for 30 min at room temperature in 120 μL of Reporter Lysis Buffer. Luciferase activity was measured by a luminescence assay, and a protein assay was performed using a Micro BCA Protein Assay Reagent Kit. 10 μL of the lysate was dispensed into a luminometer tube, and luciferase activity was integrated over 10 s with a 2 s measurement delay in a Lumat LB 9507 luminometer (Berthold, Germany) with an automatic injection of 50 μL of luciferase assay reagent. The final results were reported in terms of RLU/mg cellular protein.

Fluorescence Miscroscopy. HeLa cells were seeded at a density of 2×10^4 cells/well in a 24-well plate in a medium containing 10% FBS. The cells were treated with polyplex solution containing 2 μg of plasmid DNA (pEGFP-N3) at different weight ratios for 4 h at 37 °C. After exchange of medium, cells were further incubated for 24 h, and the fluorescence of expressed GFP was viewed using Axiovert 25 microscopy (Carl Zeiss, Germany). The images were obtained using *AxioVision 3.1* software.

Treatment with Inhibitors. HeLa cells were seeded at a density of 1×10^5 cells/well in a 24-well plate. After 1 day of incubation in normal conditions, cells were pretreated with genistein (200 μM) (*18*), wortmannin (100 nM) (*19*), or chlorpromazine (10 μg/mL) (*20*) for 1 h, or chloroquine (100 μM) for 30 min, before addition of polyplexes. Genistein is reported to inhibit caveolae-mediated uptake processes, and chlorpromazine is known to block clathrin-mediated endocytosis. Wortmannin is an inhibitor of phosphatidyl inositol-3-phosphate (PI3) kinase completing macropinocytosis, and chloroquine is well-known to inhibit endosome acidification. Polyplexes of PPP5 and PPP5-R, containing 2 μg of plasmid DNA, were prepared at weight ratios of 15 and 10, respectively. After 2 h of polyplex incubation, all media were washed with PBS and replaced with fresh media containing 10% serum, then cells were further incubated for 2 days before assay.

Potassium Depletion. HeLa cells were seeded at a density of 1×10^5 cells/well in a 24-well plate and treated with a procedure described by Larkin et al., which results in rapid depletion of cellular potassium (*21*). Potassium depletion of the cells is known to perturb clathrin-mediated endocytosis. After 1 day of incubation in normal conditions, cells were rinsed with K^+-free buffer (140 mM NaCl, 20 mM Hepes, 1 mM $CaCl_2$, 1 mM $MgCl_2$, 1 mg/mL D-glucose; pH 7.4) and subsequently rinsed for 5 min with hypotonic buffer (K^+-free buffer diluted 1:1 with distilled water), followed by washing three times with K^+-free buffer. Control cells were treated with buffer (K^+-free buffer + 10 mM KCl). Polyplexes were incubated with the cells for 2 h and washed with PBS. Then, all media were replaced with fresh media containing 10% serum, and cells were further incubated for 2 days before assay.

RESULTS AND DISCUSSION

Synthesis and Characterization of PPP5-R. Backbone polymer, PAMAM-PEG-PAMAM G5 (PPP5), was synthesized according to the previous report (*6*). The synthesis of PPP5 was monitored by ^{1}H NMR spectroscopy. Arginine conjugation of PPP5 was performed with the HOBt/HBTU coupling method in DMF. Fmoc groups of conjugated arginines were removed by piperidine solution, and the reagent (95:2.5:2.5, trifluoroacetic acid/triisopropylsilane/water, v/v) was used to deprotect the pbf groups of coupled arginines. Scheme 1 shows the entire synthetic procedure of PPP5-R. The synthesis of PPP5-R was confirmed by ^{1}H NMR spectroscopy and MALDI-TOF. The ^{1}H NMR spectra is shown in Figure 1.

The number of grafted arginines was calculated by comparing the NMR peak intensities between the protons of PEG and arginine. Approximately 36 molecules of arginine were found to be conjugated to 1 molecule of PPP5. From this result, the molecular weight of PPP5-R was calculated to be 2.37×10^4 Da. Meanwhile, the Mn and Mw of PPP5-R were experimentally measured using MALDI-TOF. Figure 2 shows the MALDI-TOF MS of PPP5-R. 1:1 DHB/fucose mixture, a well-known "cold" matrix was used as a matrix (*22*). The Mn was estimated to be 2.34×10^4 Da and the Mw to be 2.37×10^4 Da. The polydispersity index of the polymer was determined to be 1.01. The MALDI-TOF result was found to correspond well with the ^{1}H NMR result.

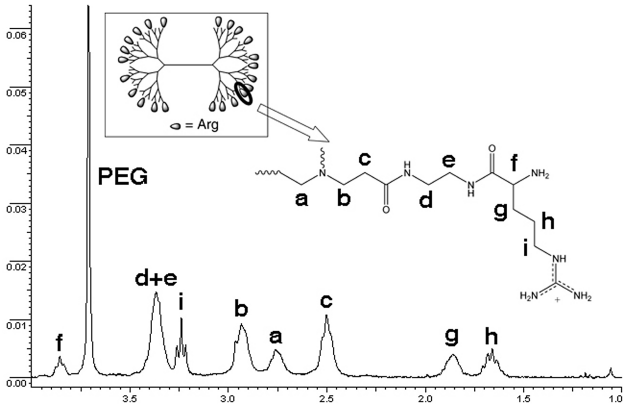

Figure 1. ^{1}H NMR spectra of PPP5-R in D_2O. Molecule in box represents PPP5-R.

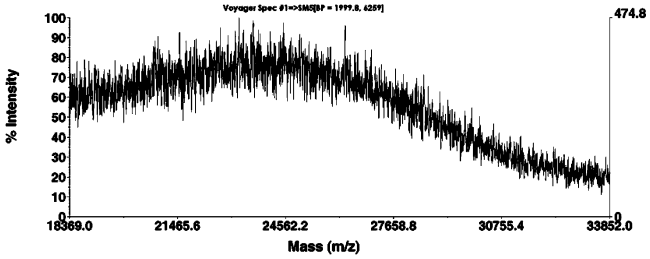

Figure 2. MALDI-TOF MS of PPP5-R.

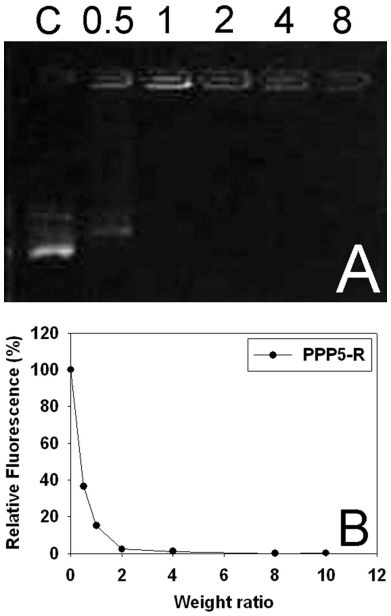

Figure 3. (a) Agarose gel retardation of PPP5-R polyplexes. The numbers represent the weight ratios of the polyplexes. C: plasmid DNA only. (b) PicoGreen reagent assay of PPP5-R polyplexes. Values were represented as relative fluorescence (%) to the value of plasmid DNA.

Self-Assembly of PPP5-R and Plasmid DNA. The self-assembly of PPP5-R and plasmid DNA was examined by agarose gel retardation assay and PicoGreen reagent assay, respectively. PicoGreen reagent is a highly sensitive probe for monitoring polymer/DNA self-assembly (*23*). Figure 3a shows the gel retardation assay result of PPP5-R. PPP5-R could retard the migration of plasmid DNA by forming polyplexes at a weight ratio of 1. Nonmigration of DNA in the gel indicates condensation of DNA by PPP5-R. In a PicoGreen reagent assay experiment (Figure 3b), the polymer is thought to possess a strong DNA condensing ability, as the relative fluorescence intensity of polyplex is abruptly decreased to 15% at a weight ratio of 1 and even to 2% at a ratio of 2.

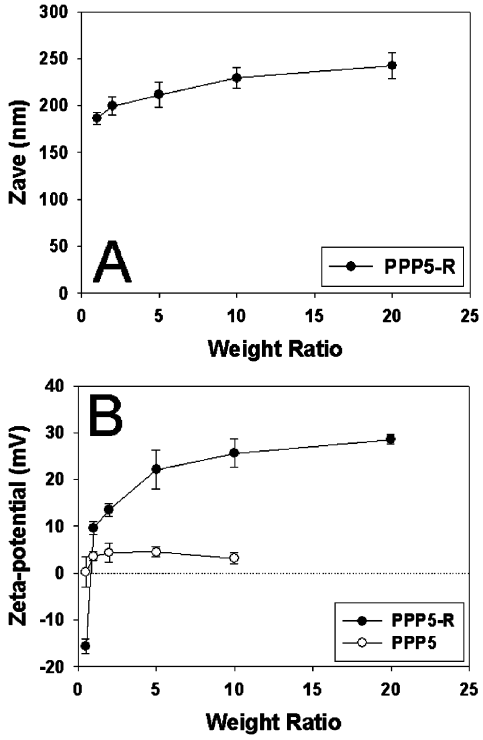

Figure 4. (a) Average size measurements of PPP5-R polyplexes. (b) ζ-Potentials of PPP5-R and PPP5 polyplexes.

Size and ζ-Potential Measurements of the PPP5-R Polyplexes. The proper size of polyplexes is thought to be essential for efficient gene delivery. We performed the average size measurements of PPP5-R polyplexes using a Zeta-sizer. Polyplexes were prepared at various weight ratios ranging from 1 to 20. As shown in Figure 4a, the average size of the polyplexes was 186 nm at a weight ratio of 1 and gradually increased to 242 nm at 20. A plateau of size values from a weight ratio of 5 indicated the formation of stable polyplexes with a size appropriate for gene delivery.

The ζ-potential values of the polyplexes were also estimated at various weight ratios ranging from 0.5 to 20 using a Zeta-sizer (Figure 4b). We also performed ζ-potential measurements for native PPP5 polyplexes to analyze the effect of the arginine modification of PPP5. The positive potential value of the polyplex is thought to be important to adhere to the negatively charged cellular membrane, leading to the intracellular uptake of the polyplex. The ζ-potential value of PPP5-R polyplex was negative (−15.6 mV) at a weight ratio of 0.5 and abruptly increased to 9.7 mV at a ratio of 1. In addition, the values were around 22−28 mV at the ranges over weight ratio 5, displaying stable complex formation with plasmid DNA. On the other hand, the ζ-potential values of PPP5 polyplex were around 3−5 mV even at a weight ratio of 10. In addition, we have reported an interesting result about the ζ-potential experiments of dendritic

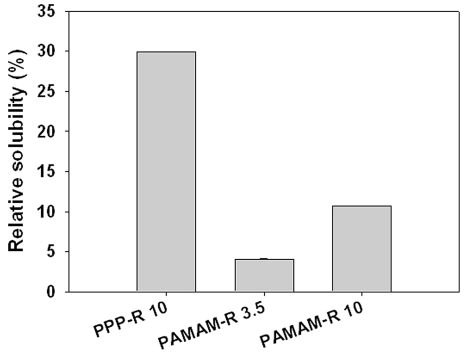

Figure 6. Water solubility of PPP5-R polyplex. The numbers represent the weight ratios of the polyplexes.

triblock copolymer, poly(L-lysine) dendrimer-PEG-poly(L-lysine) dendrimer (PLLD-PEG-PLLD) (*24*). The potential value of PLLD-PEG-PLLD polyplex did not rise to a positive value even at a charge ratio of 8, suggesting that two PLL dendrimer blocks located at each end of the copolymer self-assemble with DNA, and accordingly, the surface of the polyplex is coated with hydrophilic PEG chains. There are big differences in the pK_a value of surface functionalities and molecular size of the dendritic blocks of each block copolymer. The pK_a value of guanidine group of arginine residue is over 12, although that of the primary amine of PLLD and PAMAM is about 10. So, the dendritic blocks of PPP5-R would possess stronger positive charges than others at the same pH condition. Moreover, the molecular weights of the dendritic block of $PLLD_4$-PEG-$PLLD_4$, PPP5, and PPP5-R are about 1920, 6760, and 10 590, respectively. Therefore, it is thought that large dendritic blocks with high positive charges may not be fully shielded by PEG chains even after PEG-coated complexation.

Atomic Force Microscopy (AFM). The morphologies of PPP5-R polyplexes were observed by AFM. Polyplexes were prepared at various weight ratios ranging from 0.5 to 10. As shown in Figure 5a, PPP5-R could not condense plasmid DNA compactly, and so DNA stretched out from hundreds of nanometer-scale semicondensed polyplex cores like a corona at a weight ratio of 0.5. At a ratio of 1, the polymer could condense plasmid DNA to a complex, but we could still observe the small projections around the core, which were inferred to be a portion of noncondensed plasmid DNA (Figure 5b). At a ratio of 10, it was observed that PPP5-R could form compact spherical polyplexes with plasmid DNA with homogeneity and about a 200-nm size (Figure 5c). These results agreed well with the size measurement results obtained by Zeta-sizer.

Water Solubility. After complexation, some polyplexes show a tendency to aggregate in water because of increased hydrophobicity caused by charge neutralization, limiting their in vivo application (*5*). So, we examined the water solubility of the PPP5-R polyplex. PAMAM-R G4 was used as a control reagent because its molecular structure was identical to that of PPP5-R

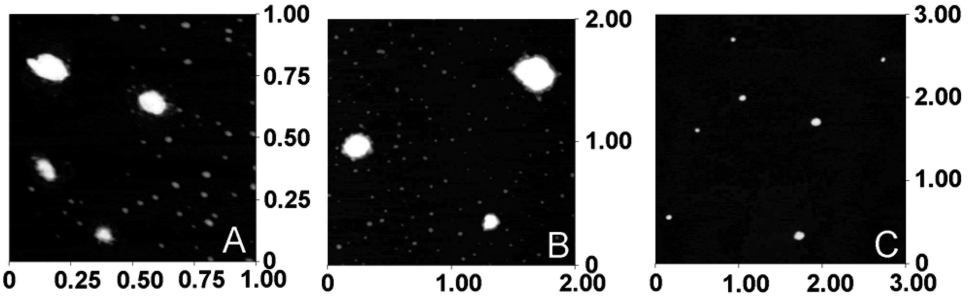

Figure 5. AFM images of PPP5-R polyplexes: at weight ratios of (a) 0.5, (b) 1, and (c) 10. The numbers around the figures represent μm-scaled sizes.

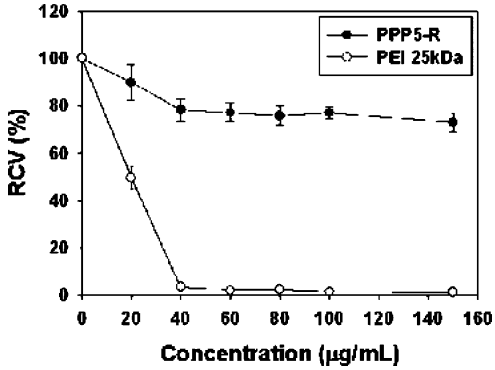

Figure 7. Cytotoxicity of PPP5-R in HepG2 cells by MTT assay. RCV: relative cell viability. Data were expressed as mean ± standard deviation ($n = 5$).

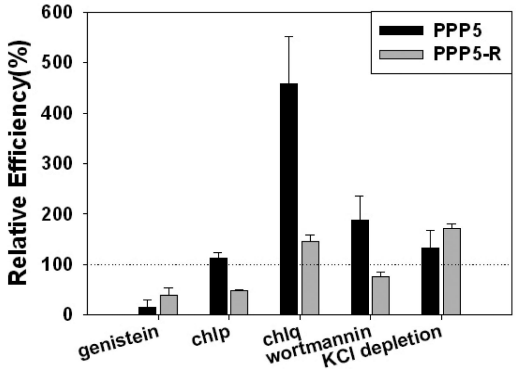

Figure 9. Relative transfection efficiency (RTE) of each polyplex in treating various cellular uptake inhibitors and in potassium depletion condition. chlp , chlorpromazine; chlq, chloroquine; RTE = experimental value/control value × 100 (%). Data were expressed as mean ± standard deviation ($n = 3$).

except the core part. As shown in Figure 6, we can find that PPP5-R polyplex has a sixfold enhanced water solubility compared to PAMAM-R G4 polyplex in an optimal ratio for transfection. From this result, it is obvious that the PEG core of PPP5-R plays an important role for increasing the water solubility of the polyplex.

Cytotoxicity. The cytotoxicity of PPP5-R was examined on HepG2 cell lines by MTT assay. PEI was used as a control. The cytotoxicity of PEI is well-known. As shown in Figure 7, cell viability of PEI was 50% at 20 μg/mL and decreased to 4% at 40 μg/mL of concentration, while PPP5-R displayed 77−90% cell viability in the same concentration range, suggesting that the cytotoxicity of PPP5-R is minimal.

Transfection Experiments. Transfection efficiency of PPP5-R was examined on HeLa, C2C12, and HepG2 cells. PEI was used as a control reagent in optimal condition. PPP5-R showed very high transfection efficiency comparable to that of PEI in the presence or absence of serum in HeLa and C2C12 cells in Figure 8a,b. The transfection efficiencies of both PEI and PPP5-R were observed to be reduced in the presence of serum. Interestingly, transfection efficiency ratios (+FBS/−FBS) of PEI were 0.03 and 0.07 in C2C12 and HeLa cells, respectively, while the ratios of PPP5-R were in a range between 0.10 and 0.23. Considering our previous data for native PPP5 (transfection efficiency ratio = 0.85−1.3) (*6*), the PEG core of the copolymers is thought to coat the surface of the polyplex and inhibit the nonspecific interaction of polyplexes with serum compartments, suppressing the reduction of the transfection efficiency. However, in the case of PPP5-R, PEG could not coat the polyplex completely, reducing its efficiency ratio, as described in the ζ-potential experiment. The transfection efficiency of PPP5-R was also compared with that of native PPP5 on HepG2 cells (Figure 8c). PPP5-R showed a transfection efficiency value 20−36 times higher than that of native PPP5.

Furthermore, we can also identify a much increased transfection activity of PPP5-R in fluorescence microscopy. A considerable number of cells expressed green fluorescence protein in treatment with PPP5-R/pEGFP polyplex (Figure 8e), unlike with PPP5/pEGFP polyplex (Figure 8d). This greatly increased transfection efficiency of PPP5-R must be due to the arginine residues grafted onto the periphery. From these results, we hypothesize that arginine residues of PPP5-R would function

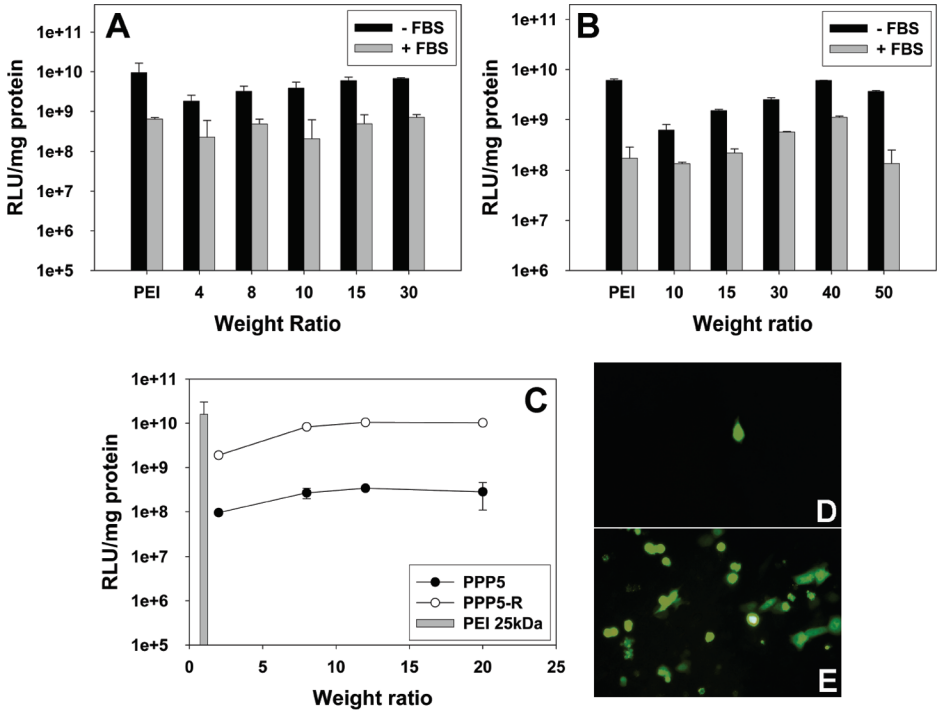

Figure 8. Transfection experiments in (a) HeLa cells, (b) C2C12 cells, and (c) HepG2 cells. PEI and PPP5 are used as control reagents. (d,e) represent GFP expression in HeLa cells by PPP5 and PPP5-R, respectively. Data were expressed as mean ± standard deviation ($n = 3$).

Scheme 2. Schematic Diagram of the Proposed Cellular Uptake Mechanism of PPP5 Polyplex and PPP5-R Polyplex

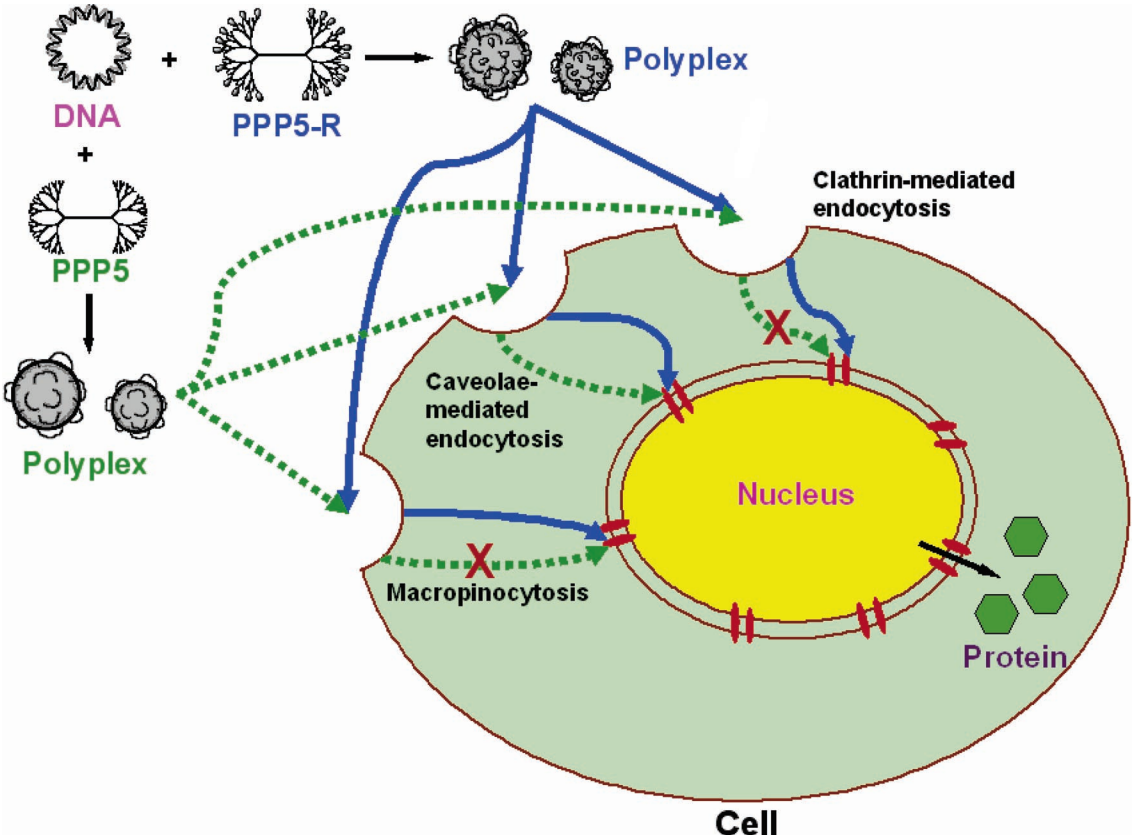

as a key to a cellular membrane gate, which guides the PPP5-R polyplex to the cellular uptake pathway for efficient transfection.

Cellular Uptake Pathway Leading to Enhanced Transfection. These transfection results raise a question about the differences of the cellular uptake pathway leading to enhanced transfection between native PPP5 and arginine-grafted PPP5-R. The cellular uptake pathway of cell-penetrating peptides containing Tat sequences and oligo-arginine peptides has been reported by many groups (*13*−*15*), but that of arginine-grafted dendritic polymer polyplex is not well-understood. We performed the transfection experiments on HeLa cells by treatment with various cellular uptake inhibitors and compared the effect in order to examine the cellular uptake pathway leading to effective transfection of PPP5 and PPP5-R polyplexes, for the first time. Genistein is reported to inhibit caveolae-mediated uptake processes (*18*), and chlorpromazine is known to block clathrin-mediated endocytosis (*20*). Wortmannin is an inhibitor of phosphatidyl inositol-3-phosphate (PI3) kinase completing macropinocytosis (*19*), and chloroquine is a well-known endosome acidification inhibitor.

Figure 9 represents the relative transfection efficiencies of PPP5 and PPP5-R polyplexes in the presence of each inhibitor. In the case of PPP5, only genistein reduced the efficiency considerably, and chlorpromazine did not affect the efficiency. The result suggests that PPP5 polyplexes entering through caveolae-mediated uptake lead the effective transfection and agrees well with the other report (*25*). In the presence of chloroquine, its enhanced efficiency leads us to believe that the cellular uptake of PPP5 polyplex also happens through clathrin-mediated endocytosis but the polyplex may not escape from the endosome efficiently, not leading to effective transfection. It is thought that chloroquine helps the PPP5 polyplex escape from the endosome by inhibiting acidification of the endosome and leading to mechanical swelling of the polymer. This view is well-supported by the previous result that the transfection efficiency of PPP5 is relatively lower in HepG2 cells lacking caveolin-1 than in 293 cells (*6*). Macropinocytosis inhibition by treatment with wortmannin led to a somewhat increased transfection efficiency of PPP5 polyplex. It is thought that this may be associated with the fact that the cellular uptake of polyplex through macropinocytosis is reported to impair the transfection efficiency (*19*).

Interestingly, unlike with PPP5, the transfection of the PPP5-R polyplex is reduced in the presence of both genistein and chlorpromazine by 39% and 47%, respectively, and is not particularly affected in the presence of chloroquine. This result represents evidence that the effective transfection of arginine-grafted dendritic polymer is carried out through the cellular uptake of both caveolae- and clathrin-mediated pathways to some degree. A relatively small effect of chloroquine on PPP5-R in comparison with PPP5 and the inhibition of transfection by chlorpromazine suggest that PPP5-R polyplex may have its own specific competency to escape from the compartments of a clathrin-dependent pathway, unlike PPP5 polyplex. Macropinocytosis inhibition by wortmannin reduced the transfection efficiency by 76%, unlike in the recent report by Nakase et al. that the cellular uptake of arginine-rich peptides was significantly suppressed by a macropinocytosis inhibitor (*26*). Our results show that arginine-rich peptide and arginine-grafted dendritic copolymer polyplex have distinct internalization mechanisms. Scheme 2 shows the proposed cellular uptake mechanisms leading to transfection of both PPP5 polyplex and PPP5-R polyplex.

Moreover, we performed the transfection experiments of both polyplexes in the depletion of potassium ion in order to confirm the chlorpromazine experimental result (Figure 9). Potassium depletion of the cells is also known to perturb clathrin-mediated endocytosis (*21*). In line with our expectations, the transfection of PPP5 polyplexes was not affected by potassium depletion, which corresponded with the chlorpromazine result. However, on the contrary, the transfection efficiency was increased about twofold in the case of PPP5-R. Discordance with the previous

chlorpromazine result leads us to preconclude that another factor could be affecting the cellular uptake of arginine-grafted dendritic polymer. Recently, Rothbard et al. reported that the membrane potential of cells strongly induces the translocation of guanidinium-rich peptides, and the membrane potential is related to the negative log value of the concentration ratio of extracellular (K_o) and intracellular (K_i) potassium ions (*27*). In KCl-containing buffer, generally K_o and K_i are known to be about 10 mM and 140 mM, respectively. In potassium depletion condition, K_o may become a micromolar concentration at most and K_i drops to 40% (about 50 mM) when polyplex solution is added after about 15 min of cell rinsing (*21*). According to Rothbard et al.'s formula, the membrane potential would become more negative in the potassium depletion condition, and it may induce more cellular uptake of polyplexes and the following enhanced transfection efficiency.

In summary, these results strongly suggest that the cellular uptake leading to the effective transfection of arginine-grafted dendritic polymer polyplex is not dependent on one exclusive pathway and has the possibility of combination of multiple pathways, unlike with the caveolae-dependent uptake of PPP5 polyplex lacking arginine residues. Therefore, this unique uptake mechanism of the PPP5-R polyplex is thought to be one of the important reasons for the enhanced transfection efficiency of the polyplex. Moreover, we are studying the nuclear localization ability of the arginine residues, which may provide another key explanation for the result. This finding would help us to understand arginine-based polymeric gene carriers and to develop more efficient gene delivery carriers in the future.

Finally, PPP5-R would be a less toxic and high transfection efficient gene delivery carrier unrelated to cell type because of its multiple uptake mechanisms. Also, it would show the potential for drug delivery systems by conjugation of drugs to the polymer due to its great cell-penetrating ability.

CONCLUSION

We synthesized a novel arginine-grafted dendritic block copolymer, R-PAMAM-PEG-PAMAM-R G5 (PPP5-R), for gene delivery systems. PPP5-R could form nanosized polyplexes with plasmid DNA, which was examined by agarose gel electrophoresis, PicoGreen reagent assay, Zeta-sizer, and AFM. The positive ζ-potential values of the PPP5-R polyplex show the formation of positively charged stable polyplex particles and suggest that large dendritic blocks with high positive charge may not be fully shielded by PEG chains even after PEG-coated complexation. The PPP5-R polyplex showed enhanced water solubility due to the PEG core and low cytotoxicity. The PPP5-R polyplex represented the greatly enhanced transfection efficiency in comparison with native PPP5 on various cell lines. By treating various cellular uptake inhibitors, we concluded that the cellular uptake leading to the effective transfection of arginine-grafted dendritic polymer PPP5-R polyplex is not dependent on one exclusive pathway and has the possibility of multiple pathways, unlike with the caveolae-dependent uptake of PPP5 polyplex lacking arginine residues. Moreover, this particular cellular uptake pathway of PPP5-R is proposed to be one of the important reasons for the enhanced transfection efficiency.

ACKNOWLEDGMENT

This work was supported by the Korea Health 21 R&D Project of The Ministry of Health & Welfare, Republic of Korea (A04-0004), the Gene Therapy Project of the Ministry of Science and Technology (M1053403004-05N3403-00410), and the KBRDG Initiative Research Program (F104AD010011-06A0401-01110).

LITERATURE CITED

(1) Kay, M. A., Liu, D., and Hoogerbrugge, P. M. (1997) Gene therapy. *Proc. Natl. Acad. Sci. U.S.A. 94*, 12744−12746.

(2) Luo, D., and Saltzman, W. M. (2000) Synthetic DNA delivery systems. *Nat. Biotechnol. 18*, 33−37.

(3) Zauner, W., Ogris, M., and Wagner, E. (1998) Polylysine-based transfection systems utilizing receptor-mediated delivery. *Adv. Drug Delivery Rev. 30*, 97−113.

(4) Veena, V., Thomas, T., and Thomas, T. J. (2002) DNA nanoparticles and development of DNA delivery vehicles for gene therapy. *Biochemistry 41*, 14085−14094.

(5) Tang, M. X., and Szoka, F. C., Jr. (1997) The influence of polymer structure on the interactions of cationic polymers with DNA and morphology of the resulting complexes. *Gene Ther. 4*, 823−832.

(6) Kim, T.-i., Seo, H. J., Choi, J. S., Jang, H. S., Baek, J. U., Kim, K., and Park, J. S. (2004) PAMAM-PEG-PAMAM: Novel triblock copolymer as a biocompatible and efficient gene delivery carrier. *Biomacromolecules 5*, 2487−2492.

(7) Brooks, H., Lebleu, B., and Vivès, E. (2005) Tat peptide-mediated cellular delivery: back to basics. *Adv. Drug Delivery Rev. 57*, 559−577.

(8) Zhao, M., and Weissleder, R. (2004) Intracellular cargo delivery using Tat peptide and derivatives. *Med. Res. Rev. 24*, 1−12.

(9) Wadia, J. S., and Dowdy, S. F. (2005) Transmembrane delivery of protein and peptide drugs by TAT-mediated transduction in the treatment of cancer. *Adv. Drug Delivery Rev. 57*, 579−596.

(10) Tung, C.-H., and Weissleder, R. (2003) Arginine containing peptides as delivery vectors. *Adv. Drug Delivery Rev. 55*, 281−294.

(11) Sen, J., and Chaudhuri, A. (2005) Design, syntheses, and transfection biology of novel non-cholesterol-based guanidinylated cationic lipids. *J. Med. Chem. 48*, 812−820.

(12) Choi, J. S., Nam, K., Park, J.-y., Kim, J.-B., Lee, J.-K., and Park, J.-s. (2004) Enhanced transfection efficiency of PAMAM dendrimer by surface modification with L-arginine. *J. Controlled Release 99*, 445−456.

(13) Richard, J. P., Melikov, K., Vivès, E., Ramos, C., Verbeure, B., Gait, M. J., Chernomordik, L. V., and Lebleu, B. (2003) Cell-penetrating peptides. A reevaluation of the mechanism of cellular uptake. *J. Biol. Chem. 278*, 585−590.

(14) Fischer, R., Kohler, K., Fotin-Mleczek, M., and Brock, R. (2004) A stepwise dissection of the intracellular fate of cationic cell-penetrating peptides. *J. Biol. Chem. 279*, 12625−12635.

(15) Fittipaldi, A., Ferrari, A., Zoppe, M., Arcangeli, C., Pellegrini, V., Beltram, F., and Giacca, M. (2003) Cell membrane lipid rafts mediate caveolar endocytosis of HIV-1 Tat fusion proteins. *J. Biol. Chem. 278*, 34141−34149.

(16) Kim, T.-i., Seo, H. J., Choi, J. S., Yoon, J. K., Baek, J.-u., Kim, K., and Park, J.-S. (2005) Synthesis of biodegradable cross-linked poly(β-amino ester) for gene delivery and its modification, inducing enhanced transfection efficiency and stepwise degradation. *Bioconjugate Chem. 16*, 1140−1148.

(17) Wadhwa, M. S., Knoell, D. L., Young, A. P., and Rice, K. G. (1995) Targeted gene delivery with a low molecular weight glycopeptide carrier. *Bioconjugate Chem. 6*, 283−291.

(18) Liu, P., and Anderson, R. G. (1999) Spatial organization of EGF receptor transmodulation by PDGF. *Biochem. Biophys. Res. Commun. 261*, 695−700.

(19) Goncalves, C., Mennesson, E., Fuchs, R., Gorvel, J.-P., Midoux, P., and Pichon, C. (2004) Macropinocytosis of polyplexes and recycling of plasmid via the clathrin-dependent pathway impair the transfection efficiency of human hepatocarcinoma cells. *Mol. Ther. 10*, 373−385.

(20) Wang, L. H., Rothberg, K. G., and Andrson, R. G. (1993) Mis-assembly of clathrin lattices on endosomes reveals a regulatory switch for coated pit formation. *J. Cell Biol. 123*, 1107−1117.

(21) Larkin, J. M., Brown, M. S., Goldstein, J. L., and Anderson, R. G. (1983) Depletion of intracellular potassium arrests coated pit

formation and receptor-mediated endocytosis in fibroblasts. *Cell 33*, 273−285.

(22) Gusev, A. I., Wilkinson, W. R., Proctor, A., and Hercules, D. M. (1995) Improvement of signal reproducibility and matrix/comatrix effects in MALDI analysis. *Anal. Chem. 67*, 1034−1041.

(23) Singer, V. L., Jones, L. J., Yue, S. T., and Haugland, R. P. (1997) Characterization of PicoGreen reagent and development of a fluorescence-based solution assay for double-stranded DNA quantitation. *Anal. Biochem. 249*, 228−238.

(24) Choi, J. S., Joo, D. K., Kim, C. H., Kim, K., and Park, J. S. (2000) Synthesis of a barbell-like triblock copolymer, poly(L-lysine) dendrimer-*block*-poly(ethylene glycol)-*block*-poly(L-lysine) dendrimer, and its self-assembly with plasmid DNA. *J. Am. Chem. Soc. 122*, 474−480.

(25) Rejman, J., Bragonzi, A., and Conese, M. (2005) Role of clathrin- and caveolae-mediated endocytosis in gene transfer mediated by lipo- and polyplexes. *Mol. Ther. 12*, 468−474.

(26) Nakase, I., Niwa, M., Takeuchi, T., Sonomura, K., Kawabata, N., Koike, Y., Takehashi, M., Tanaka, S., Ueda, K., Simpson, J. S., Jones, A. T., Sugiura, Y., and Futaki, S. (2004) Cellular uptake of arginine-rich peptides: roles for macropinocytosis and actin rearrangement. *Mol. Ther. 10*, 1011−1022.

(27) Rothbard, J. B., Jessop, T. C., Lewis, R. S., Murray, B. A., and Wender, P. A. (2004) Role of membrane potential and hydrogen bonding in the mechanism of translocation of guanidinium-rich peptides into cells. *J. Am. Chem. Soc. 126*, 9506−9507.

BC0601525